Received: 22 December 2025 | Accepted: 24 June 2026

DOI: 10.1111/syen.70066

ORIGINAL ARTICLE

Systematic Entomology | Royal Entomological Society

# Evolution and biogeography of the widespread dragonfly genus *Orthetrum* (Odonata: Anisoptera: Libellulidae): Massive dispersal in the tertiary

Violet Onsongo[1] | John C. Abbott[2] | Seth M. Bybee[3] | Klaas-Douwe B. Dijkstra[4] | Paul B. Frandsen[5] | Aaron Goodman[1,6] | Robert Guralnick[7] | Vincent J. Kalkman[4] | Manpreet Kohli[1,8] | Lacie Newton[1,9] | Lorenzo Prendini[1] | Christopher J. Raxworthy[10] | Jessica Ware[1]

[1]Division of Invertebrate Zoology, American Museum of Natural History, New York, New York, USA

[2]The University of Alabama Museums Research & Collections, The University of Alabama, Tuscaloosa, Alabama, USA

[3]Department of Biology and Monte L. Bean Museum of Natural History, Brigham Young University, Provo, Utah, USA

[4]Naturalis Biodiversity Center, Leiden, The Netherlands

[5]Department of Plant and Wildlife Sciences and Bean Life Science Museum, Brigham Young University, Provo, Utah, USA

[6]Department of Entomology, University of Illinois at Urbana Champaign, Urbana, Illinois, USA

[7]Florida Museum of Natural History, University of Florida, Gainesville, Florida, USA

[8]Department of Natural Sciences, Baruch College, City University of New York, New York, New York, USA

[9]Department of Biological Sciences, New Jersey Institute of Technology, Newark, New Jersey, USA

[10]Division of Vertebrate Zoology, American Museum of Natural History, New York, New York, USA

**Correspondence**
Violet Onsongo, Division of Invertebrate Zoology, American Museum of Natural History, New York, NY 10024, USA.
Email: vonsongo@amnh.org

**Funding information**
U.S. National Science Foundation (NSF), Genealogy of Odonata (GEODE): Dispersal and Color as Drivers of 300 Million Years of Global Dragonfly Evolution, Grant/Award Numbers: Abbott: 2002489, Ware: 2002473, Bybee: 2002432, Guralnick: 2002457

**Editor:** Bonnie Blaimer

## Abstract

With 67 species, *Orthetrum* Newman is the most speciose genus within the family Libellulidae Leach (Odonata: Anisoptera), distributed across the Afrotropical, Palearctic, Indo-Malayan, Malagasy, Oceania, Wallacea and Australasian regions. Despite its wide distribution, serving as a top predator in freshwater ecosystems, the evolutionary history of *Orthetrum* has remained unresolved, with prior studies limited to morphology and sparse genetic sampling (<33% of species). We present here the most comprehensive phylogenetic study of *Orthetrum* to date, sampling 50 of 67 species (~75%) using Anchored Hybrid Enrichment (AHE). Our analyses, integrating concatenated maximum likelihood and coalescent-based approaches, provide a robust, strongly supported phylogeny that confirms the monophyly of *Orthetrum* and reveals four distinct clades. Two clades comprise mostly Afrotropical species, whereas the remaining clades are from the Palearctic, Indo-Malayan, Oceania, Wallacea and Australasian regions. Divergence time estimates indicate that *Orthetrum* originated ~32 million years ago, with major diversification

occurring from ~28 Ma onward, well after major continental fragmentation events. Ancestral range reconstruction under the best supported Dispersal–Extinction–Cladogenesis (DEC) framework does not support a single-region origin; instead, early lineages are inferred to have occupied a broadly connected Afro–Eurasian system. Subsequent diversification is characterized by stepwise dispersal across adjacent regions, including repeated expansions into the Indo-Malayan and Palearctic regions, followed by colonization of Australasia, Wallacea and Oceania. The Afrotropical region emerges as a major centre of lineage persistence and diversification, with subsequent range expansion in some lineages during the early Miocene (~23 Ma), whereas Madagascar reflects at least five independent colonization events from Africa resulting in endemic species.

**KEYWORDS**
anchored hybrid enrichment, monophyletic clades, phylogenetic relationships, skimmer dragonflies, systematics

## INTRODUCTION

The genus *Orthetrum* Newman is the largest genus within the family Libellulidae Leach, commonly known as skimmers (Paulson et al., 2024). Species of *Orthetrum* are widely distributed across the Afrotropical, Palearctic and Indo-Malayan regions, with extensions into Australasia, occupying a broad diversity of freshwater habitats, including forest streams, desert pools, bogs and occasionally brackish environments such as salt marshes (Dijkstra, 2025). Within these systems, they are especially common and often dominant in both flowing (lotic) and standing (lentic) waters, including temporary habitats such as shallow seasonal ponds (Boudot et al., 2020; Dijkstra & Clausnitzer, 2014; Dumont & Verschuren, 2005; Khelifa et al., 2013; Wildermuth, 2008; Zhang, 2019). Like many other dragonflies, they play a crucial role as top predators in aquatic ecosystems, helping to maintain the ecological balance and serving as indicators of environmental health (Oertli, 2008; Farkas et al., 2012; Zhang, 2019). The genus *Orthetrum* contains 67 species (Paulson et al., 2024) found in the Afrotropical, Palearctic, Indo-Malayan, Malagasy, Oceania, Wallacea and Australasian biogeographic regions (Paulson et al., 2024), with nearly half recorded from the Afrotropicals (Dijkstra & Kalkman, 2012).

Their colouration varies depending on species, developmental stage and sex. Mature males usually have vibrant colours, with most having a bluish thorax and abdomen, due to a waxy pruinosity. Females and immature males are yellow to brown (see Figure 1). In a few species, the males have a bright red or purple thorax and abdomen (Subramanian et al., 2018; Zhang, 2019).

Although *Orthetrum* is widely distributed across the Eastern Hemisphere and ubiquitous in freshwater ecosystems, its evolutionary history remains poorly resolved. No densely sampled phylogenetic study has rigorously tested the validation of its monophyly, and interspecific relationships within the genus remain unclear. Previous work on the systematics of *Orthetrum* and other Odonata has relied largely on morphological characters for species identification and classification (Corbet, 1999; Dijkstra & Kalkman, 2012; Dijkstra et al., 2014; Paulson, 2009), with only a few molecular studies available (Lalțanpuii et al., 2014; Yong et al., 2014, 2016). These molecular studies have been limited in both marker choice and taxon sampling: Lalțanpuii et al. (2014) analysed a single mitochondrial gene fragment [403 bp of cytochrome oxidase I (COI)], Yong et al. (2014) used a combination of mitochondrial and nuclear markers across six species (*O. chrysis*, *O. sabina*, *O. testaceum*, *O. luzonicum*, *O. glaucum* and *O. pruinosum*), and Yong et al. (2016) generated complete mitochondrial genomes for a small subset of taxa. Although Lalțanpuii et al. (2014) included 22 species, substantial overlap exists among studies, and the total number of unique species sampled remains limited to ~22 of the 67 currently recognized species (~33%) (Paulson et al., 2024). This limited sampling has hindered the resolution of phylogenetic relationships and constrained our understanding of diversification and biogeographic patterns within the genus.

In addition, several species complexes within *Orthetrum* are notoriously difficult to distinguish based solely on morphology and are suspected to include cryptic diversity, such as the reddish *O. chrysis* Selys, *O. testaceum* Burmeister and the bluish *O. glaucum* Brauer, *O. chrysostigma* Burmeister and *O. luzonicum* Brauer (Clausnitzer et al., 2009; Zhang, 2019). Molecular data are therefore essential for resolving these complex relationships. Furthermore, given the widespread distribution of the genus, biogeographic analyses are necessary to evaluate the relative roles of dispersal and vicariance in shaping its diversification across regions.

To address these knowledge gaps, this study had three primary aims. First, we reconstructed a robust phylogeny of the genus *Orthetrum* by generating a large genomic dataset (~20 kb) using the Anchored Hybrid Enrichment (AHE) approach (Bybee et al., 2021; Goodman et al., 2023; Goodman et al., 2025a; Goodman et al., 2025b; Lemmon et al., 2012; Tolman et al., 2023; Ware et al., 2025). This dataset, largely derived from museum specimens, comprises targeted nuclear and mitochondrial loci (~92 loci) sampled across a broad representation of species. Second, we estimated divergence times to establish a temporal framework for the origin and diversification of the genus. Third, we investigated the biogeographic

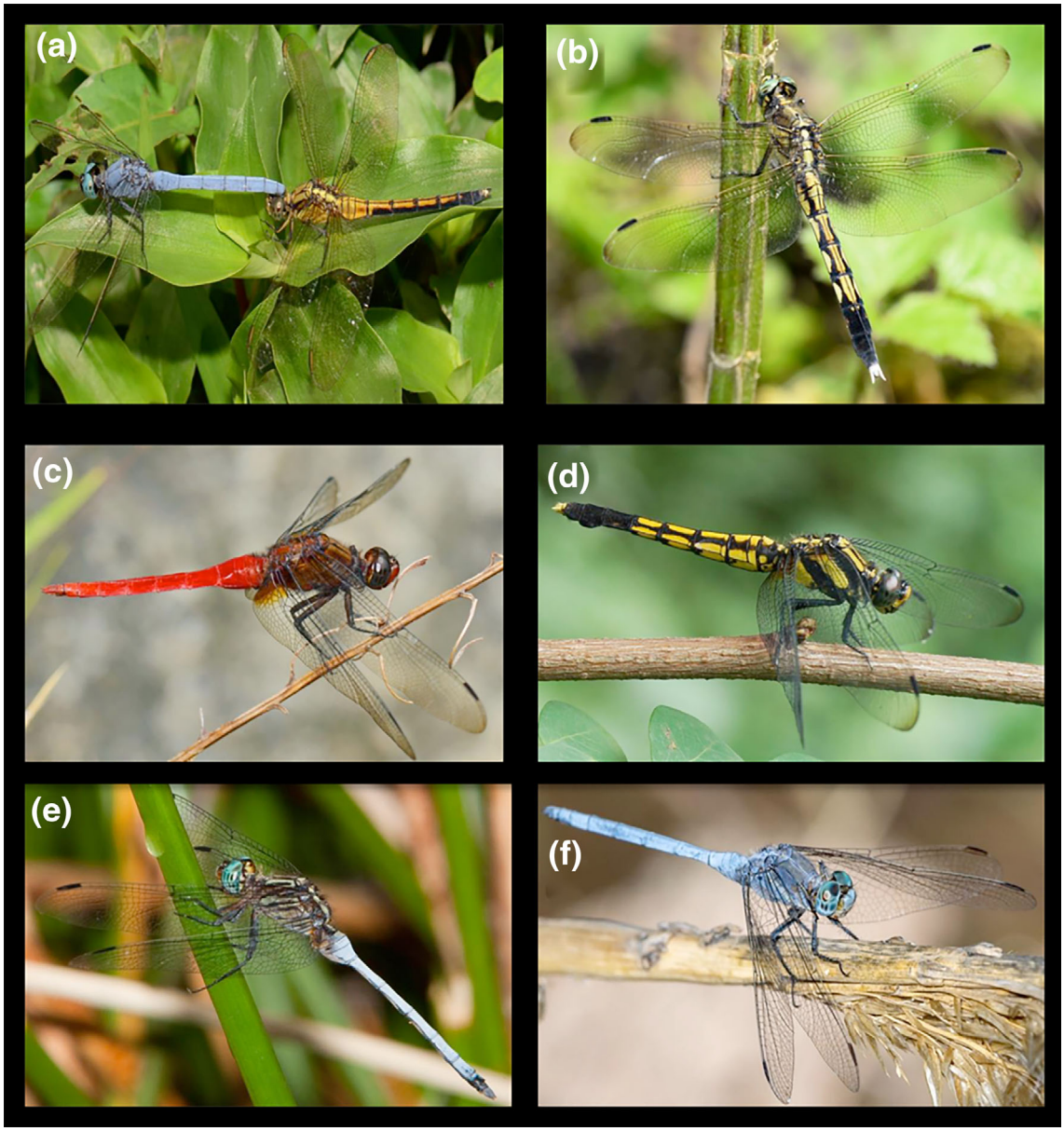


**FIGURE 1** Diversity of *Orthetrum* Newman species: (a) *Orthetrum luzonicum*, Brauer male (bluish) and female (brownish); (b) *Orthetrum albistylum*, Selys male; (c) *Orthetrum Chrysis* Selys male; (d) *Orthetrum melania* Selys female; (e) *Orthetrum julia* Kirby; and (f) *Orthetrum chrysostigma* Burmeister male (bluish). Photos provided by John Abbott and Haomiao Zhang.

history and diversification dynamics of *Orthetrum*, with a particular focus on assessing the relative roles of dispersal and regional connectivity in shaping its present-day distribution.

## MATERIALS AND METHODS

### Taxon sampling

Taxa were sampled as part of the 'Genealogy and Ecology of Odonata (GEODE)' grant, and hence specimens were given 'GEODE' alphanumeric codes, and/or alphanumeric codes related to the collections from which they were sampled (Table S1). *Orthetrum* specimens were acquired from the Florida State Collection of Arthropods (FSCA) and the Naturalis Biodiversity Center [Rijksmuseum of Natuurlijke Historie (RMNH)]. All specimens used in this study were obtained from existing museum collections. No new field collections were conducted as part of this study. Specimens were originally collected under the appropriate permits and regulations in their respective countries of origin. Therefore, no additional collecting authorizations were required for this research. The taxon sampling includes 50 species of the 67 species (75%) known worldwide (Paulson et al., 2024). Following Newton et al. (2026), five outgroup species, *Nesciothemis minor* (RMNH30232917), *Nesciothemis nigeriensis* (RMNH4000477573), *Plathemis subornata* (GEODE7708), *Ladona julia* (GEODE7735) and *Oxythemis phoenicosceles*, were selected based on their close phylogenetic relationship to the ingroup and used to root the phylogeny. All specimen provenance data are provided in Table S1.

In addition, we assessed the 17 *Orthetrum* species not included in our molecular dataset. Although these taxa were not sequenced, available biogeographic and morphological information (Table S2) was used to infer their potential phylogenetic placement relative to the 50 species analysed here.

## DNA extraction and sequencing

Genomic DNA was extracted from a single hind leg excised from each specimen that had been dried and stored in glassine envelopes. Leg tissue excision was performed using sterilized forceps to minimize contamination. DNA extractions were conducted utilizing a Zymo kit from Zymo Research 2011 Micro-prep kit protocols (Hilden, Germany), generally following the manufacturer's protocols with minor modifications. These included extending the incubation period up to 10 days to enhance tissue digestion; to minimize potential loss of DNA, we reduced the number of wash steps involving the g-DNA wash buffer, and DNA was eluted in 100 μL of buffer instead of 50 μL. DNA concentration and quality were assessed using a Qubit 4 Fluorometer (Thermo Fisher Scientific). DNA yields from historical museum specimens were variable, as expected for aged and often degraded material, and ranged from 40 to 1550 ng/μL, corresponding to total DNA yields of approximately 3.2–155 μg per sample. Despite this broad range in concentration, DNA quality varied substantially among samples, with some exhibiting degradation typical of historical material. Accordingly, samples with lower DNA quantity and/or quality were processed using a low-input library preparation protocol to improve sequencing success.

All DNA extracts were submitted to RAPID Genomics (Gainesville, Florida, USA) for library preparation. Libraries were sequenced on an Illumina HiSeq 2500 platform using the AHE Odonata probe set following Bybee et al. (2021) and Goodman et al. (2023). Probe sets were designed by scanning 941 exons similarly shared across insects using published data from 24 odonates transcriptomes (Futahashi et al., 2015; Suvorov et al., 2017) and also two assembled genomes from Bybee et al. (2021). In addition, 211 functional loci were sequenced, focusing on vision, flight and immunity (Bybee et al., 2021; Goodman et al., 2023). We sequenced one representative species per genus using the full targeted set of 1306 probe sets (500 kb), while a reduced set of ~92 loci (20 kb) was targeted for broader taxon sampling across the dataset (see Table S3). Raw AHE sequencing reads have been deposited in the NCBI Sequence Read Archive (SRA) under BioProject accession (PRJNA1475513). The assembled loci and associated datasets are available through the Dryad Digital Repository: https://doi.org/10.5061/dryad.4f4qrfjtf (Data S1). Locus recovery assigned accession numbers and coverage statistics for each species are provided in the Table S3.

## AHE assembly and analysis

The raw sequence data were processed and analysed on the MENDEL HPC Cluster at the American Museum of Natural History. We used fastp (Tang & Wong, 2001) to remove adapters from the raw reads of each sample and assessed the quality using multiQC (Ewels et al., 2016). We implemented a slightly modified pipeline from Breinholt et al. (2018) to assemble and attribute orthology to each targeted capture locus. Briefly, we individually assembled each locus with iterative baited assembly with SPAdes v. 3.15.5 (Prjibelski et al., 2020). We identified orthologs by querying the target probe set against the assembled scaffolds using the TBLASTX algorithm from BLAST+ v.2.15.0 (Camacho et al., 2009), which we confirmed by ensuring that the scaffold and associated probe hit to the same location in the reference genome *Tanypterx hageni*, Seys (Tolman et al., 2023). We only kept the best reciprocal hit between each assembled sequence and the reference genome to ensure that each locus was single copy (i.e., we removed any potential paralogs).

## Phylogenetic analysis

We conducted a multiple sequence alignment for each locus with the MAFFT-linsi algorithm in MAFFT v.7.475 (Katoh & Standley, 2013). Prior to alignment, loci represented by fewer than four taxa were removed. Such sparsely sampled loci often contain little or no overlapping sequence data, which can lead to alignment instability and errors during both array-based processing and downstream concatenation. Each alignment was trimmed using a 0.75 threshold cutoff (i.e., only loci with 75% minimum completeness were retained) using TrimAL v1.4.1 (Capella-Gutiérrez et al., 2009), and subsequently each alignment was checked manually in AliView v1.28 (Larsson, 2014) to ensure all regions were well aligned. We concatenated the alignment using FASconCAT v1.11 (Kück & Meusemann, 2010). Each AHE locus was initially treated as a separate partition, resulting in locus-based partitioning of the concatenated dataset, and we then used the relaxed clustering with the model fixed to GTR + G for each initial partition to identify an optimal partitioning scheme in IQtree v2.1.3 (Minh et al., 2020). We then selected the best nucleotide substitution model for each subset in the partitioning scheme using ModelFinder and estimated a maximum likelihood (ML) tree. We estimated branch support using 1000 ultrafast bootstrap replicates (UFboot) in IQtree v2.1.3 (Kalyaanamoorthy et al., 2017). To ensure that our phylogenetic inference was not influenced by incomplete lineage sorting (ILS), we reconstructed maximum-likelihood (ML) trees for each locus with 1000 UFboot and inferred a coalescent species tree from the unrooted gene trees using ASTRAL-III v.5.6.1 with local posterior probabilities (LPPs) as support values (Zhang et al., 2018). To further assess the potential impact of ILS and introgression, we calculated gene concordance factors (gCFs) and site concordance factors (sCFs) in IQ-TREE2 (Minh et al., 2020), which quantify the proportions of gene trees and informative sites supporting each bipartition in the ML tree.

## Divergence time estimation

Divergence times were estimated using a node-dating approach and secondary calibrations in MCMCtree as implemented in the software

package PAML v.4.7a (Yang, 2007). Due to the absence of reliable fossil calibrations within *Orthetrum*, temporal constraints were derived from the recent phylogenomic framework of Newton et al. (2026), which incorporates 22 fossil calibrations and extensive taxon sampling (i.e., ~67% of genera represented) to estimate divergence times across Odonata. Although secondary calibrations can propagate uncertainty from prior analyses, their use here is justified because the source study provides a robust, fossil-calibrated temporal framework directly relevant to the clades examined. To further minimize potential bias and improve transparency, we explicitly tested the sensitivity of divergence time estimates to calibration choice by implementing alternative calibration schemes.

The phylogenetic topology used for dating was visualized and edited in FigTree (Rambaut, 2014) and rooted using appropriate outgroup taxa (*Plathemis*, *Ladona*, *Oxythemis* and *Nesciothemis*) (Newton et al., 2026). Branch lengths were transformed using the 'equal' option to generate a topology suitable for approximate likelihood analysis, and the tree was exported in Newick format in FigTree (Rambaut, 2014). All branch length annotations were subsequently removed to retain topology only, allowing *mcmctree* to estimate divergence times during analysis. Fossil calibration bounds were applied as soft minimum and maximum age constraints using the standard MCMCtree notation ('>.lower<.upper') embedded directly in the Newick tree inserted immediately following the closing parenthesis of each constrained node. Placement of calibrations was verified through iterative inspection of the tree to ensure correspondence with the intended clades.

Two alternative calibration schemes were implemented to evaluate the influence of the crown-node calibration on temporal inference. In the first scheme, the crown node of *Orthetrum* was constrained to 23.59–34.18 Ma following the fossil-calibrated estimate of Newton et al. (2026). Additional constraints were applied to the node encompassing all outgroups (27.88–34.18 Ma) and to the crown of Libellulinae (34.18–89.5 Ma), also based on Newton et al. (2026). In the second scheme, the *Orthetrum* calibration was excluded, and only the deeper nodes (outgroup and Libellulinae) were constrained using the same bounds. This dual-calibration framework allowed explicit testing of whether ingroup calibration influenced divergence time estimates or whether temporal inference was primarily driven by deeper, well-supported nodes.

The independent-rates relaxed-clock model was employed (clock = 2), with branch rate variation modelled using a lognormal prior. A Birth–Death–Sampling process was specified as the time prior (birth = 1, death = 1, sampling = 0). Priors were specified as rgene_gamma = G(2,2) for the overall substitution rate, sigma2_gamma = G(1,10) for the rate-drift parameter, kappa_gamma = G(6,2) for the transition/transversion ratio and alpha_gamma = G(1,1) for the among-site rate variation parameter. A soft upper bound of 89.5 Ma was applied to the root age.

For each calibration scheme, four independent Markov chain Monte Carlo (MCMC) analyses were performed to assess convergence and consistency across runs. Initial exploratory analyses (RUN_1 and RUN_2) were conducted using random seeds of 12,345 and 67,890, respectively. These runs employed a burn-in of 5000 samples, a sampling frequency of every two generations, and retained 1000,000 samples. Final analyses (RUN_3 and RUN_4) were performed using random seeds of −1 and −2, respectively, with a burn-in of 50,000 samples, a sampling frequency of every 50 generations, and retention of 100,000 posterior samples see Data S3. Posterior estimates and summary statistics were calculated from the two final runs after confirming convergence among independent analyses. Convergence was assessed by comparing posterior likelihoods, divergence-time estimates and model parameters among independent runs and by examining trace files in Tracer v1.7.2 (Rambaut et al., 2018). Independent runs converged on nearly identical posterior estimates and overlapping 95% highest posterior density intervals, indicating satisfactory convergence and mixing.

Comparison of the two calibration schemes showed highly similar divergence time estimates. Excluding the *Orthetrum* crown calibration scheme resulted in only modest increases in node ages (approximately 5%–6% for the crown node of *Orthetrum*), indicating that temporal inferences were robust to calibration choice and were largely informed by the deeper fossil-calibrated nodes. Because the *Orthetrum* calibrated scheme incorporated direct temporal information for the focal clade while producing results consistent with the alternative calibration strategy, the posterior mean chronogram from the *Orthetrum* calibrated RUN_4 analysis was used for downstream ancestral area reconstruction and biogeographic analyses.

## Biogeographical analysis

Ancestral range reconstruction in *Orthetrum* was inferred using BioGeoBEARS in the R package BioGeoBears v1.1.2 (Matzke, 2013a, 2013b) using our time-calibrated phylogeny from the *Orthetrum* calibrated RUN_4 analysis. Analyses were conducted on the time-scaled phylogeny of *Orthetrum* excluding outgroup taxa, with geographic ranges coded across seven biogeographic regions: Afrotropical (A), Indo-Malayan (B), Palearctic (C), Australasia (D), Oceania (E), Wallacea (F) and Malagasy (G). Assignments of extant species to these areas followed the regional distributions compiled by Kalkman et al. (2022) (map in Figure 4 and Table S1). Species occurrence data were compiled into a presence–absence matrix, where each taxon was assigned to one or more regions based on known distributions. This matrix was converted into PHYLIP/LAGRANGE format, in which each taxon is represented by a binary string indicating presence (1) or absence (0) across regions (Matzke, 2013a, 2013b; Ree & Smith, 2008). Taxon names in the geographic dataset were standardized to match those in the phylogenetic tree to ensure compatibility during likelihood calculations (Matzke, 2013a, 2013b).

We used BioGeoBEARS to reconstruct ancestral ranges because it provides a flexible likelihood-based framework for comparing alternative biogeographic models and testing different evolutionary scenarios. It allows the inclusion of the founder-event speciation parameter (+J), which models long-distance 'jump dispersal' at

speciation events (Matzke, 2013a, 2013b), a process relevant for highly dispersive taxa such as dragonflies. We evaluated three models: Dispersal–Extinction–Cladogenesis (DEC) (Ree & Smith, 2008); DIVALIKE (Ronquist, 1997); and BAYAREALIKE (Matzke, 2013a, 2013b), each with and without the +J parameter. Although the use of +J has been debated (Ree & Sanmartín, 2018), recent work supports its validity under information-theoretic model comparison (Matzke, 2022). Accordingly, we compared all models using AICc to assess alternative biogeographic scenarios and the potential role of founder-event dispersal in shaping the evolutionary history of *Orthetrum*.

We first conducted ancestral range estimation under an unconstrained state space using BioGeoBEARS, allowing all combinations of geographic regions up to the maximum observed range size = 6. This baseline analysis captures the full empirical distribution of extant taxa but is prone to inferring unrealistically widespread ancestors, particularly in clades with recent diversification. Indeed, unconstrained reconstructions frequently suggested large composite ancestral ranges spanning multiple biogeographic realms, patterns that are difficult to reconcile with Miocene palaeogeography and the ecology of modern *Orthetrum* species.

To mitigate these issues, we secondly implemented a biologically informed constraint on state space, restricting allowable ancestral ranges to those consistent with known paleogeographic connectivity over the last ~40 Myr. We defined two principal dispersal corridors: (1) a western Afro-Eurasian corridor (Afrotropical–Indo-Malayan–Palearctic; A, B, C and their combinations); (2) an eastern Indo-Australasian corridor (Australasia–Oceania–Wallacea; D, E, F and their combinations); and (3) Malagasy (G) treated as a distinct, largely isolated region. Intermediate combinations within each corridor (e.g., AB, ABC; DE, DEF) were retained to preserve the contiguity assumptions of DEC-like models, which require that transitions between areas proceed via incremental range expansion. By excluding implausible cross-corridor combinations while retaining biologically realistic intermediates, this approach balances computational tractability with paleogeographic realism. A key challenge in constrained analyses is the representation of widespread taxa. *Orthetrum sabina*, which occupies a broad distribution across Afro-Eurasian and Indo-Australasian regions (ABCDEF), exceeds the maximum allowable range size under the constrained framework and violates the assumption of geographically coherent ancestral states. To address this, we conducted sensitivity analyses in which *O. sabina* was alternatively recoded as a western range (ABC) and an eastern range (DEF). Thereby forcing the species into a single biogeographically coherent corridor in each analysis. These alternative codings were analysed under identical model conditions, allowing explicit evaluation of how the treatment of widespread taxa influences model fit and ancestral range inference.

The best-fitting model was selected based on a combination of Akaike information criterion, corrected (AICc), Akaike weights and biological plausibility following Burnham & Anderson (2004). Ancestral range reconstructions were interpreted primarily from the best-supported model, while alternative models were used to assess the robustness of inferred biogeographic patterns.

# RESULTS

## AHE data collection and phylogenetic analysis

A total of 1093 AHE loci were recovered in the 75% completeness data matrix, with 1012 loci retained after filtering loci with fewer than four taxa. The final concatenated alignment comprised 1,047,301 nucleotide sites across 58 taxa, with approximately 0.91% missing data. Of these, 97,863 were parsimony-informative sites, 228,543 were singleton sites, and 720,895 were constant sites. Locus recovery per taxon range was 90–1008 (see Table S3).

## Evolutionary relationships

In our study, the concatenated ML and coalescent-ASTRAL tree topologies were comparable in support, both producing well-resolved phylogenetic hypotheses and recovering similar overall topologies that consistently supported the monophyly of *Orthetrum* (see Figures 2 and 3). gCFs and sCFs revealed substantial variation in phylogenetic concordance across the tree. Following common practice, we considered values below 30% to indicate 'low concordance', values between 30% and 60% to indicate 'moderate concordance', and values above 60% to indicate 'high concordance'. Under these criteria, high concordance was primarily observed for shallow nodes and species-level relationships, whereas many deeper relationships within *Orthetrum* exhibited low to moderate concordance despite receiving strong bootstrap support (see Table S4).

### Australasian-Palearctic clade

This clade includes eleven *Orthetrum*: *O. albistylum*, *O. balteatum*, *O. caledonicum*, *O. cancellatum*, *O. boumiera*, *O. internum*, *O. japonicum*, *O. poecilops*, *O. trinacria*, *O. sabina* and *O. serapia* were recovered in the Australasian-Palearctic Clade with 100% bootstrap support (1.0 LPP, 37% gCF and 39.9% sCF).

### Indo-Malayan clade

This clade includes ten *Orthetrum*: *O. borneense*, *O. brunneum*, *O. chrysis*, *O. glaucum*, *O. melania*, *O. migratum*, *O. pruinosum*, *O. testaceum*, *O. triangulare* and *O. villosovittatum*, *which* were recovered in the Indo-Malayan clade with 100% bootstrap support (1.0 LPP, 32.6% gCF and 34.6% sCF).

### Afrotropical clade I

This clade includes ten species (twelve specimens) of *Orthetrum*: *O. brachiale*, *O. caffrum*, *O. camerunense*, *O. chrysostigma*, *O. chrysostigma* and *O. guineense*; three specimens of *O. julia*,

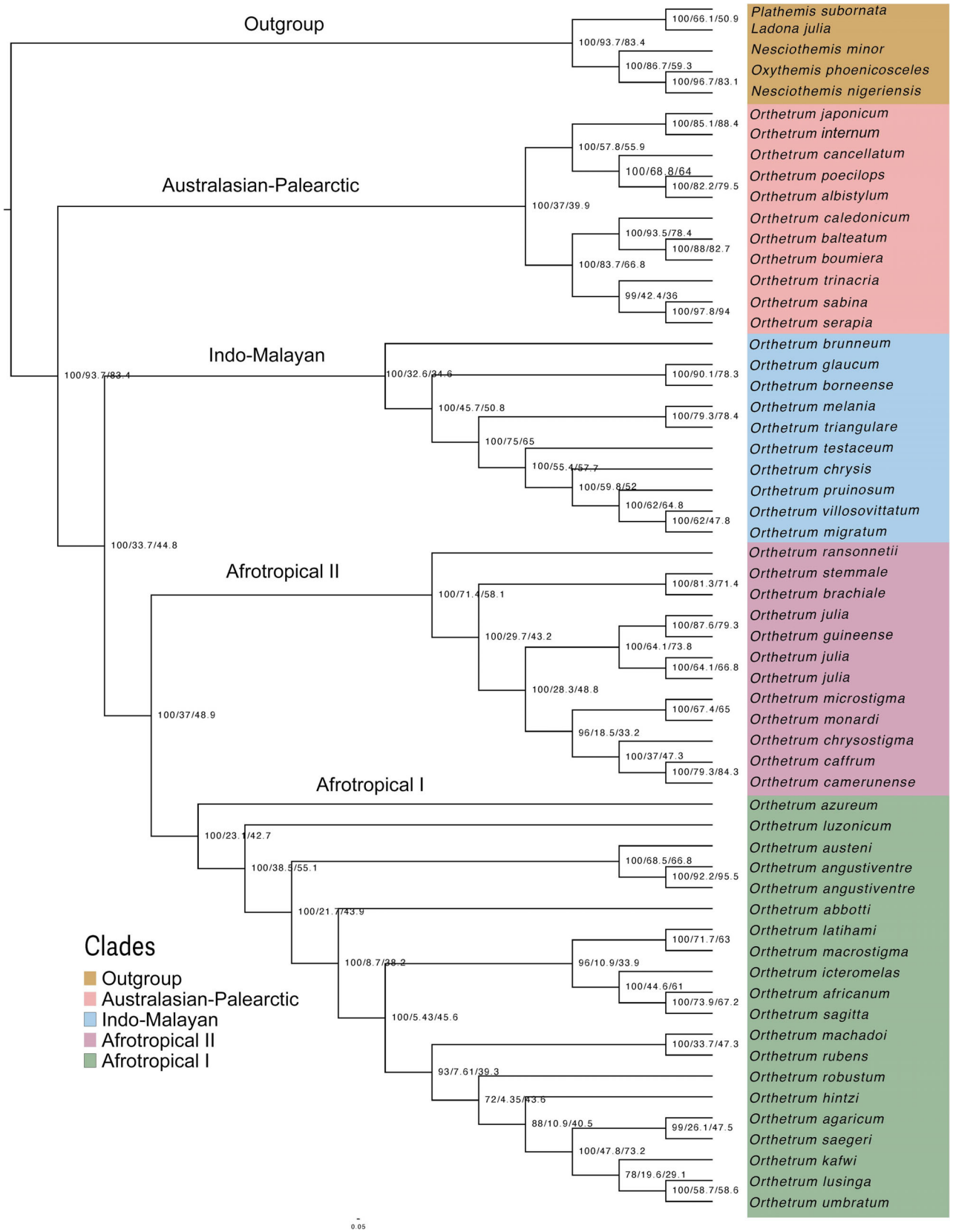


**FIGURE 2** The molecular phylogenetic tree of *Orthetrum* Newman species inferred from a maximum-likelihood analysis in IQ-TREE2. Target loci were captured using the Anchored Hybrid Enrichment (AHE) probe set described by Bybee et al. (2021). Branch labels indicate node support metrics, shown as the Ultrafast bootstrap (UFboot) support/gene concordance factor (gCF)/site concordance factor (sCF); see supplementary material Table S4. The coloured rectangle highlights the major clades recovered within *Orthetrum*.

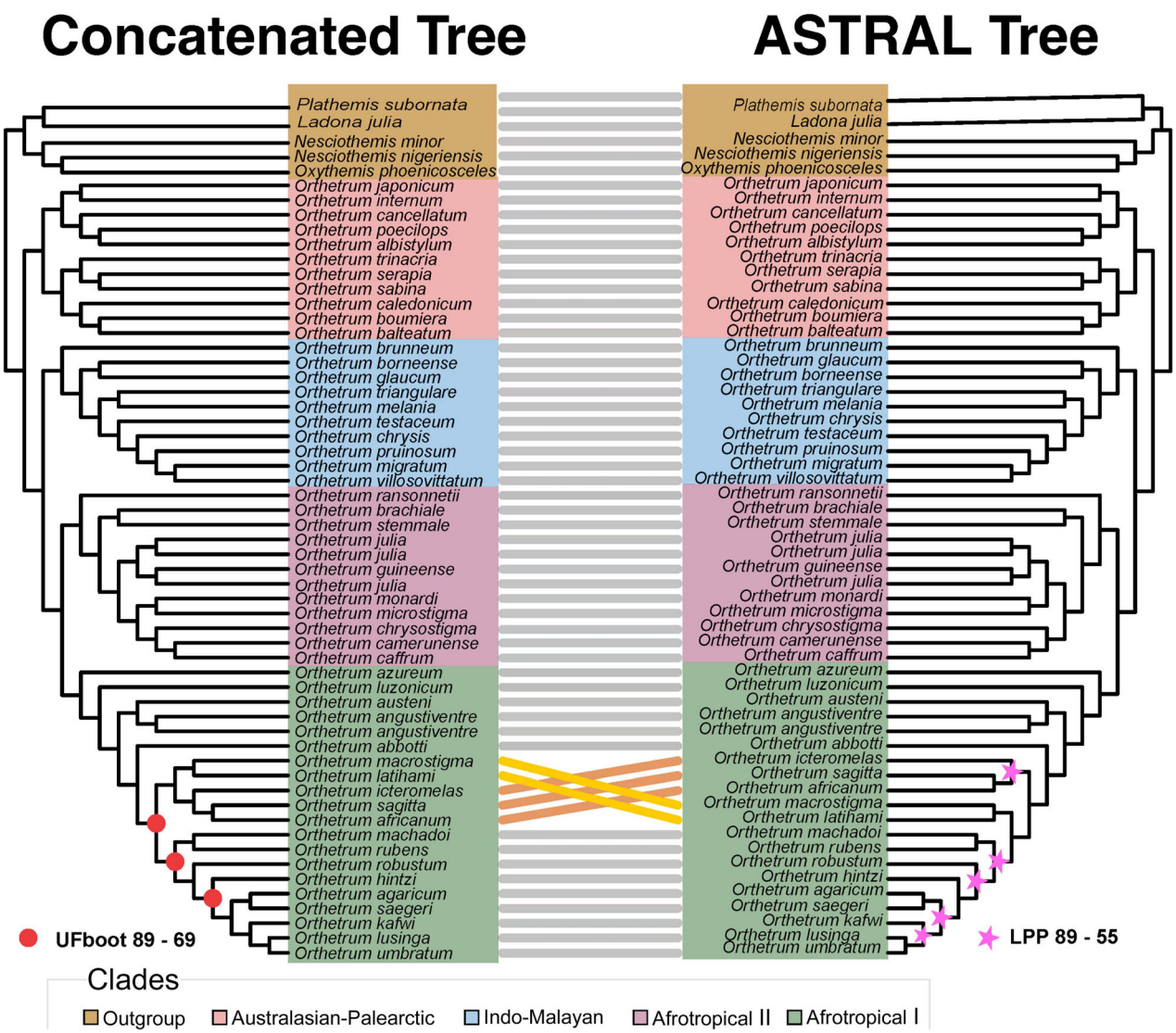


**FIGURE 3** Molecular phylogenetic relationships among *Orthetrum* Newman species inferred from nucleotide data. The left panel shows the concatenation-based maximum likelihood (ML) topology generated in IQ-TREE, and the right panel shows the coalescent-based topology inferred using ASTRAL, derived from the ultrafast bootstrap trees of each locus in the nucleotide dataset. Nodal support in the ML tree is indicated by Ultrafast bootstrap (UFboot) values, with red orange circles representing nodes supported by UFboot values of 69%–89%, and all others showing strong support (100%). Nodal support in the ASTRAL tree is represented by local posterior probabilities (LPP), where pink stars mark nodes supported by LPP values of 55–89%, and the remaining nodes exhibit strong support (100%). Horizontal coloured lines indicate the major clades recovered within *Orthetrum* in the ML topology, which are congruent with those identified in the ASTRAL topology. Coloured rectangles highlight the major clades recovered within *Orthetrum*. In the Afrotropical Clade I (green rectangle), coloured non-horizontal lines indicate topological differences between taxa in the ML and ASTRAL trees.

*O. microstigma*, *O. monardi*, *O. ransonnetii* and *O. stemmale* were recovered in the Afrotropical clade with 100% bootstrap support (1.0 LPP, 23.1% gCF and 42.7% sCF).

## Afrotropical clade II

This clade includes 20 sequences from 19 *Orthetrum* species: *O. abbotti*, two specimens of *O. angustiventre*, *O. africanum*, *O. agaricum*, *O. austeni*, *O. azureum*, *O. icteromelas*, *O. hintzi*, *O. latihami*, *O. luzonicum*, *O. kafwi*, *O. lusinga*, *O. machadoi*, *O. macrostigma*, *O. robustum*, *O. rubens*, *O. saegeri*, *O. sagitta* and *O. umbratum* were recovered in the Afrotropical clade with 100% bootstrap support (0.94 LPP, 24.2% gCF and 41.5% sCF).

The highest concordance values were observed for recent species-level divergences, such as the *O. sabina* + *O. serapia* clade (gCF = 97.8%, sCF = 94.0%) and the *O. balteatum* + *O. boumiera* + *O. caledonicum* clade (gCF = 93.5%, sCF = 78.4%). Conversely, several internal nodes within the Afrotropical lineages exhibited particularly low gCF (gCF < 15%), indicating substantial disagreement among individual gene trees. The strongest discordance was observed at several deeper nodes within the Afrotropical clades, where gCF values

ranged from 4.4% to 10.9%, reflecting extensive gene-tree conflict. Despite this low gene concordance, these nodes retained moderate sCF (sCF ≈ 33%–46%), further supporting the presence of a coherent phylogenetic signal at the site level. Together, these results suggest that localized processes such as ILS, rapid diversification or historical introgression may have contributed to discordance among loci while preserving support for the overall phylogenetic framework. Complete gCF and sCF statistics for all branches are provided in Table S4.

The ASTRAL analysis showed a normalized quartet score of 0.835, which is considered relatively high and indicates low levels of ILS, further supporting the high gCF and sCF concordance observed across the tree. The concatenated analysis showed strong ultrafast bootstrap support (100%), and the coalescence analysis had strong LPPs (1.0 LPP) along the backbone of the tree, but support values decreased at the terminal branches (see Figure S1).

## Divergence time analysis

Divergence time estimation using MCMCtree recovered a robust temporal framework for the evolution of *Orthetrum*. Scenario I (analysis without an *Orthetrum* calibration) produced consistently older age estimates than previous studies (e.g., Kohli et al., 2021; Newton et al., 2026; Suvorov et al., 2022), and we therefore present results from the scenario II (analysis with an *Orthetrum* calibration) as the primary framework, while results from scenario I can be found in the Dryad data repository accompanying this article.

The crown age of *Orthetrum* was constrained to 32 Ma (95% highest posterior density (HPD): 28–34 Ma). The earliest divergence within the genus separated the lineage containing *Orthetrum japonicum* and related taxa from the remaining species at ~29 Ma (95% HPD: 25–32 Ma), indicating early partitioning of major lineages.

Subsequent diversification of the principal clades occurred primarily during the Miocene. The Australasian-Palearctic clade (including *O. japonicum*, *O. cancellatum*, *O. albistylum* and related taxa) originated at 28 Ma (95% HPD: 25–32 Ma). The Indo-Malayan clade (including *O. brunneum*, *O. glaucum*, *O. testaceum*, *O. chrysis* and related taxa) had a crown age of 27 Ma (95% HPD: 24–31 Ma). The Afrotropical clade I, comprising species such as *O. ransonnetii*, *O. stemmale*, *O. brachiale*, *O. julia*, *O. guineense* and related taxa, was inferred to have originated at 21 Ma (95% HPD: 18–25 Ma). The second Afrotropical clade II, including *O. azureum*, *O. luzonicum*, *O. austeni*, *O. abbotti* and related species, showed a crown age of 23 Ma (95% HPD: 20–27 Ma) (see Tables 1 and S11).

Within the Afrotropical clade, the Malagasy species *Orthetrum azureum* diverged from its sister lineage at approximately 23 Ma (95% HPD: 20–27 Ma), indicating an early Miocene origin for this lineage. Terminal divergences within several species-complexes were more recent, with most species-level splits occurring during the late Miocene to Pliocene. For example, divergence between *O. angustiventre* samples was estimated at 3 Ma (95% HPD: 2–5 Ma), and the split between *O. lusinga* and *O. umbratum* at 5 Ma (95% HPD: 3–7 Ma) (Tables 1 and S11).

**TABLE 1** Divergence time estimates, 95% highest posterior density (HPD) confidence interval (CI) and geological period for selected nodes in the analysis, including the *Orthetrum* calibration.

| Node | Clade/taxon | Definition | Mean age (Ma) | 95% HPD (Ma) | Geological period |
|---|---|---|---|---|---|
| 59 | Root (full tree) | Libellulidae + outgroups | 50.8 | 39.5–64.5 | Palaeocene |
| 60 | Outgroup crown | Non-*Orthetrum* taxa | 30.1 | 27.6–33.7 | Oligocene |
| 64 | *Orthetrum* | Crown of genus | 31.9 | 28.3–34.3 | Oligocene |
| 65 | Australasian–Palearctic stem | Early *Orthetrum* split leading to the Australasian–Palearctic lineage | 28.6 | 25.2–31.9 | Oligocene |
| 66 | Australasian–Palearctic Clade crown | Australasian–Palearctic group | 23.8 | 19.9–27.9 | Oligocene |
| 70 | Australasian–Palearctic (derived) | *O. caledonicum–serapia* group | 21.5 | 17.1–25.9 | Miocene |
| 75 | Afrotropical clades (I and II) /Indo-Malayan crown-group divergence | Early *Orthetrum* split leading to the Afrotropical clades and Indo-Malayan Clade | 28.9 | 25.6–32.1 | Oligocene |
| 76 | Indo-Malayan Clade crown | Indo-Malayan–Australasian group | 27.2 | 23.8–30.6 | Oligocene |
| 85 | Crown node of the Afrotropical clades | Split of Afrotropical *Orthetrum* lineage into two major clades | 25.5 | 22.1–28.9 | Oligocene |
| 86 | Afrotropical clade I crown | Afrotropical group | 21.0 | 17.5–24.6 | Miocene |
| 97 | Afrotropical clade II crown | Afro-Indo-Malayan/Afrotropical group | 23.3 | 19.50–26.59 | Miocene |
| 98 | *O. azureum* | Stem divergence of the Madagascar lineage | 20.00 | 16.6–23.5 | Miocene |
| 101 | *O. angustiventre* | Recent divergence | 3.2 | 1.5–5.2 | Pliocene |
| 115 | *O. lusinga–umbratum* | Recent divergence | 4.6 | 2.7–6.6 | Pliocene |

*Note*: For node numbers, refer to Figure 4.

### Historical biogeography analysis

BioGeoBEARS ancestral range analyses identified the DEC model as the best-fitting model under both unconstrained (LnL = −130.89) and constrained frameworks, outperforming DIVALIKE (LnL = −135.33) and BAYAREALIKE (LnL = −136.65) (see Table S5). Under the constrained analyses, the DEF-area coded model showed a slightly improved likelihood (LnL = −128.62) relative to the ABC-area coded version (LnL = −129.39), while model ranking remained unchanged (DEC > DIVALIKE > > BAYAREALIKE; see Tables S6 and S7). Constraining the state space reduced the frequency of widespread ancestral states, although in some cases it introduced incompatibilities with the DEC transition process. For this reason, unconstrained analyses were retained as the primary basis for inference.

Ancestral range reconstructions under the DEC model (Figure 4) indicate that early nodes are associated with composite Afro–Eurasian ranges (e.g., AC, ABC), rather than a single-region origin. Subsequent nodes show a pattern of range shifts across adjacent regions, including repeated transitions into Indo-Malayan and Palearctic regions, followed by expansion into Australasia, Wallacea and Oceania.

## DISCUSSION

### Evolutionary relationships and taxonomy

Our study recovered *Orthetrum* as a monophyletic genus comprising four major clades, here designated as the Palearctic–Australasian clade, the Indo-Malayan clade, Afrotropical clade I and Afrotropical clade II (see Figure 2). The two Afrotropical clades (I and II) consist almost exclusively of Afrotropical species, whereas the Palearctic–Australasian and Indo-Malayan clades include taxa distributed across the Palearctic, Indo-Malayan and Australasian regions (see maps in Figure 4). No morphological characters are known that allow us to distinguish between the four clades, but future studies could examine characters from the secondary genitalia, for example. Within the clades, however, there are smaller groupings that can be well defined based on morphology.

The most notable patterns include a subclade within the Indo-Malayan clade comprising species with red or purple abdomens, and another subclade characterized by a spindle-shaped abdomen with a bulbous, swollen base and lacking pruinosity.

Our ASTRAL analysis reveals substantial gene tree discordance within the Afrotropical clade I, which may reflect historical hybridization, ILS or introgression events (see Figure 3). The Afrotropical clade I is characterized by short branch lengths (see the branch length tree in Figure S1) and lower bootstrap support, consistent with a potential episode of rapid radiation in its evolutionary history. Notably, this clade also exhibits topological discrepancies between the ML and ASTRAL trees, possibly indicating accelerated rates of gene evolution within the group (Mendes & Hahn, 2016). Overall, gCFs are lowest in the Afrotropical clades, further supporting the presence of discordant gene histories among its constituent taxa (see Table S4) distributed across sub-Saharan Africa. The observed genetic complexity within these clades likely reflects both their dynamic evolutionary history and ongoing diversification in the region. Recently described species, such as *O. kafwi* and *O. lusinga* from Katanga (Democratic Republic of Congo), *O. agaricum* from West Africa and *O. umbratum* from Gabon, along with their morphologically similar relatives *O. saegeri* and *O. hintzi* were included in a phylogenetic study for the first time (Dijkstra et al., 2015). Our study is the most comprehensive in terms of taxon sampling and molecular sequence data to date, providing a clear and reliable framework for the generic classification. However, species-level taxonomic uncertainties persist, particularly among the speciose African clades, highlighting the need for continued integrative taxonomic and phylogenomic investigation, especially studies on potential hybridization.

### Divergence time and historical biogeography

Our results indicate that the biogeographic history of *Orthetrum* is best explained by a dispersal-driven model of range evolution, with the DEC model consistently outperforming alternative models across analytical frameworks. Divergence time estimation places the origin of *Orthetrum* in the late Oligocene to early Miocene, with a crown age of ~32 Ma (Table 1 and Figure 4). Because diversification within the genus occurred well after major continental breakup events, vicariance is unlikely to explain present-day distributions. Instead, the temporal framework strongly supports repeated dispersal and range expansion across interconnected landmasses and island systems. The dispersal-driven patterns recovered for *Orthetrum* are consistent with broader trends observed across Odonata, where high dispersal capacity and ecological flexibility facilitate repeated intercontinental movements and regional radiations (Ware et al., 2017; Bybee et al., 2021; Goodman et al., 2024). These patterns are further supported by evidence that species richness is strongly associated with contemporary climatic conditions, particularly in warm and wet regions (Abbott et al., 2022; Cortés-Guzmán et al., 2024; Kalkman et al., 2022; Willink et al., 2024). The absence of a single-region origin, combined with the prevalence of composite Afro–Eurasian ancestral states at deeper nodes, suggests that early *Orthetrum* lineages were distributed across a geographically structured but connected system spanning the Afrotropical, Palearctic and Indo-Malayan regions. This interpretation is reinforced by divergence time estimates indicating that early lineage splits occurred during the early Miocene (~28–26 Ma), a period characterized by intermittent land connections and faunal exchange between Africa and Eurasia. Rather than representing widespread uniform distributions, these composite ancestral states likely reflect occupation of adjacent regions within a continuous or intermittently connected biogeographic network. This interpretation aligns with broader patterns observed across Odonata, where Africa plays a central role in diversification while participating in repeated biogeographic exchange with Eurasia, rather than representing a single, isolated point of origin (Dijkstra et al., 2014).

Recent phylogenomic studies emphasize the role of dispersal and faunal exchange in shaping odonate distributions across major

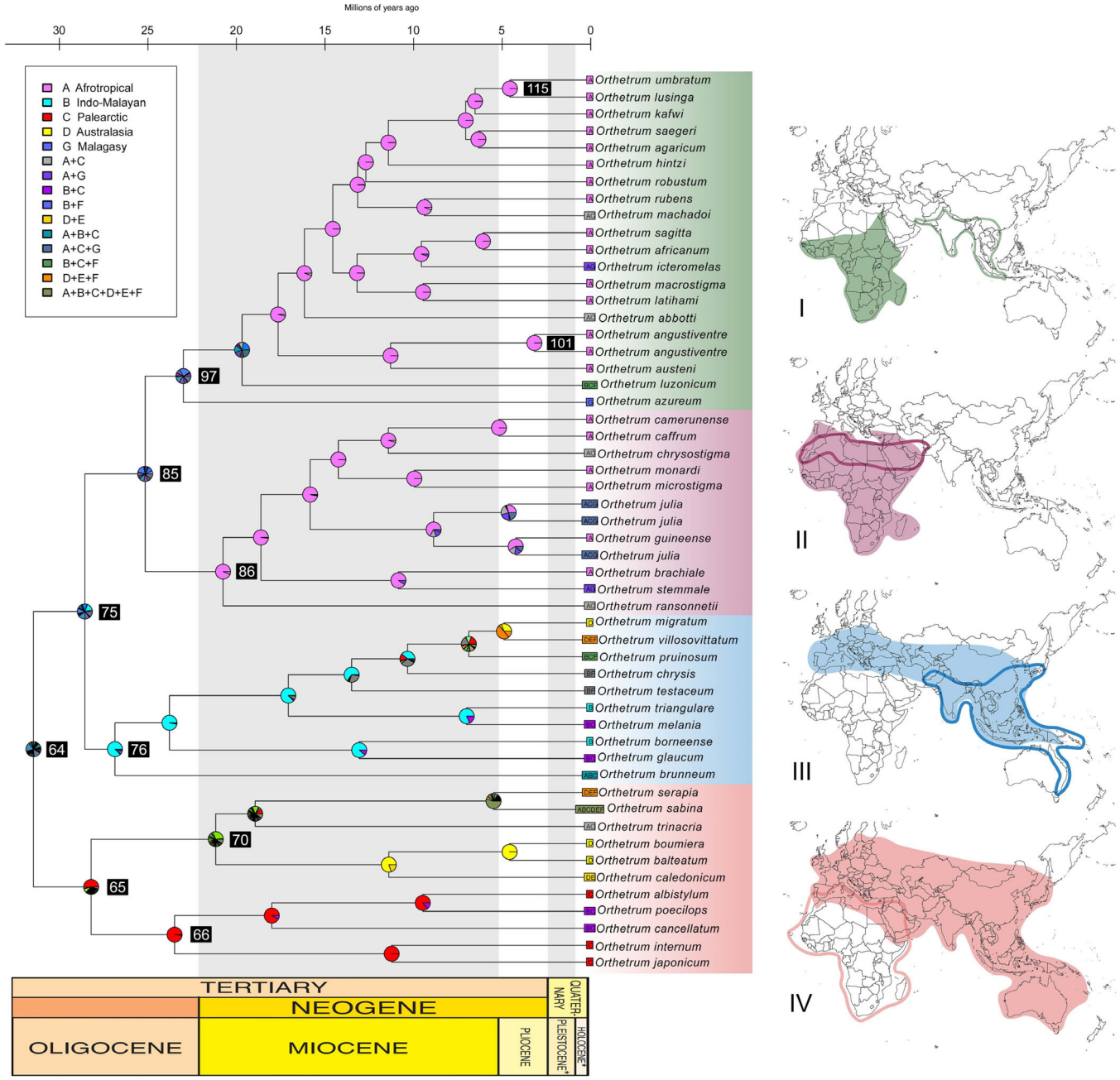


**FIGURE 4** Ancestral range reconstruction of *Orthetrum* (excluding outgroups) inferred under the dispersal–extinction–cladogenesis (DEC) model implemented in BioGeoBEARS v1.1.2 (Matzke, 2013a, 2013b). Analyses were conducted in R using our time-calibrated phylogeny from the *Orthetrum* calibrated RUN_4 analysis MCMCtree. The time-scaled phylogeny was pruned to include only *Orthetrum*, and geographic ranges were coded across seven biogeographic regions: Afrotropical (a), Indo-Malayan (b), Palearctic (c), Australasia (d), Oceania (e), Wallacea (f) and Malagasy (g). Assignments of extant species to regions follow Kalkman et al. (2022). Geographic distributions are illustrated as follows: (I) distribution of species in the Afrotropical clade I, with the range of *O. luzonicum*, the only predominantly Indo-Malayan representative, indicated by a line; (ii) distribution of species in the second Afrotropical clade II, with the range of *O. ransonnetii* indicated by a line; (III) distribution of species in the Indo-Malayan clade, with the ranges of red-abdomen *Orthetrum* species (*O. testaceum*, *O. chrysis*, *O. pruinosum*, *O. villosovittatum* and *O. migratum*) indicated by lines; and (IV) distribution of species in the Palearctic-Australasia clade, with the range of *O. trinacria*, the only Afrotropical representative, indicated by a line. Horizontal coloured bars at the tips of the phylogeny indicate the major clades recovered in the ML analysis (Figure 3). Coloured boxes denote the present-day distribution of species according to the defined biogeographic regions (Table S1). Node numbers indicate the key nodes discussed in Table 1, whereas complete information for all nodes is provided in Supplementary material Table S11. Pie charts at internal nodes represent relative probabilities of ancestral ranges inferred for each lineage.

biogeographic realms, including the Afrotropical, Palearctic, Nearctic, Indo-Malayan, Australasian and Neotropical regions, with many lineages exhibiting widespread ancestral ranges followed by stepwise colonization of adjacent regions across both the Eastern and Western Hemispheres (Ware et al., 2017; Bybee et al., 2021; Tolman et al., 2024; Hadfield et al., 2025; Goodman et al., 2025a, Goodman

et al., 2025b). Consistent with this pattern, our divergence time estimates indicate that major *Orthetrum* clades diversified primarily during the Miocene. The Indo-Malayan and Palearctic lineages originated earlier, during the late Oligocene (~28–26 Ma), whereas subsequent diversification within clades occurred primarily during the Miocene. The Indo-Malayan clade shows evidence of early expansion across a connected Afro–Eurasian system, with widespread taxa such as *O. sabina* and *O. serapia* linking Indo-Malayan, Wallacean, Oceanian and Australasian regions and *O. trinacria* and *O. azureum* indicating dispersal involving Africa and Madagascar. The Palearctic–Australasian clade diversified around ~23 Ma (95% HPD: 20–27 Ma), and the phylogenetic separation of *O. caledonicum* from the *O. balteatum*–*O. boumiera* and *O. villosovittatum*–*O. migratum* lineages supports at least three independent colonization events into Australasia, rather than a single colonization followed by radiation. This pattern is consistent with broader phylogenetic studies of insects and Odonata, which demonstrate high dispersal capacity and recurrent intercontinental movements shaping lineage distributions (Ware et al., 2017).

In contrast, the two Afrotropical clades show slightly younger origins (~21 Ma; 95% HPD: 17–24 Ma) and are largely restricted to Africa, but each exhibits evidence of secondary range expansion. One clade includes *O. ransonnetii*, reflecting dispersal into Afro–Palearctic arid systems, whereas the other includes *O. luzonicum*, indicating a later expansion into Indo-Malayan and Wallacean regions. These patterns show evidence of both outward dispersal and localized diversification, reinforcing the role of Africa as both a source region and a centre of lineage persistence (Dijkstra et al., 2014). Similarly, the biogeographic history of Madagascar reveals five Malagasy-associated colonization events, including one endemic Malagasy lineage (*O. azureum*) and four Africa–Madagascar or Afro–Eurasian–Malagasy lineages (*O. stemmale*, *O. julia*, *O. icteromelas* and *O. trinacria*), inferred to have arisen through subsequent dispersal from mainland Africa during the Miocene. These results reinforce the view that dispersal, rather than vicariance, has been a dominant process structuring biodiversity across both continental margins and oceanic islands, driving the assembly of present-day faunas through repeated cycles of colonization and diversification (Ware et al., 2017; Bybee et al., 2021; Dijkstra et al., 2014; Gillespie et al., 2012).

A key challenge in reconstructing the biogeographic history of *Orthetrum* is the presence of widespread taxa, particularly *Orthetrum sabina*, whose distribution spans six biogeographical regions. In unconstrained analyses, such taxa contribute to the inference of broad composite ancestral ranges, potentially inflating estimates of ancestral distributions. To address this, we conducted sensitivity analyses by recoding *O. sabina* into alternative biogeographically coherent states (ABC vs. DEF) (see Data S4). Although these alternative codings resulted in slight differences in likelihood, with the DEF-coded version providing a marginally better fit, the overall model ranking (DEC > DIVALIKE > > BAYAREALIKE) remained unchanged (see Tables S6 and S7). The alternative codings affected the most likely ancestral range at only a small number of deep nodes and primarily altered the probabilities assigned to widespread composite ancestral ranges. Overall, ancestral range reconstructions were highly consistent across analyses, with 47 and 48 of 52 internal nodes ABC and DEF, respectively, recovering the same most-likely ancestral state (see Tables S8–S10). Consequently, the principal biogeographic interpretation remained unchanged, indicating that our conclusions are robust to alternative representations of widespread taxa and are not driven by idiosyncratic coding decisions.

While biologically constrained analyses improved model fit by restricting unrealistic combinations of geographic regions, they also introduced mathematical incompatibilities with the transition process assumed by DEC, particularly when intermediate states required for range evolution were excluded. As a result, the constrained framework could not fully accommodate the empirical distribution data without violating model assumptions. Consequently, we retained the unconstrained analyses as the primary framework for inference (Figure 4), using constrained analyses as a complementary approach to evaluate robustness (see Data S2).

The biogeographic patterns uncovered in this study closely parallel ecological and morphological differentiation within the genus. Many *Orthetrum* species exhibit blue pruinosity, a waxy coating associated with sexual maturity and UV protection, which is advantageous for males that perch for long periods in exposed, sunlit habitats (Futahashi, 2020; Futahashi et al., 2019; Moore et al., 2024). Such adaptations are widespread across the genus and likely facilitated repeated colonization of open lowland environments throughout the Indo-Malayan and Afrotropical regions.

In contrast, the species group containing *O. sabina*, *O. serapia* and *O. trinacria* in the Australasian–Palearctic clade, all belonging to early diverging Indo-Malayan and Afrotropical lineages, did not develop blue pruinosity. Instead, these species have long, slender abdomens and high flight activity associated with predation on relatively large prey (Chathura Priyadarshana et al., 2023). Their reduced pruinosity likely reflects their ecological versatility: these species are among the most widespread and disturbance-tolerant dragonflies in tropical Asia, Australasia and Africa (Dijkstra & Clausnitzer, 2014; Kalkman et al., 2020). Behavioural thermoregulation through active patrolling may reduce the selective pressure for reflective pruinosity in these lineages (Corbet, 1999; De Marco & Resende, 2002; May, 1976).

A similar ecological signal is evident within the Indo-Malayan clade, where all red male species (*O. testaceum*, *O. chrysis*, *O. pruinosum*, *O. villosovittatum*, *O. migratum*) form a monophyletic group. In these species, males turn red with age, sometimes overlaid with partial pruinosity, yielding a purple colouration. Their behaviour of long periods spent basking at open water bodies suggests that both red pigmentation and partial pruinosity function in heat and UV management, analogous to blue pruinose taxa in other libellulid genera (Suárez-Tovar et al., 2022).

## CONCLUSIONS

Our study provides the most comprehensive phylogenetic and biogeographic assessment of *Orthetrum* to date, recovering the genus as a strongly supported monophyletic lineage with four major clades. Divergence time estimates indicate that the genus originated in the

late Oligocene to early Miocene (~32 Ma), followed by extensive diversification throughout the Miocene across Afro–Eurasian and Indo-Australian regions. The integration of divergence time and biogeographic analyses supports a dispersal-driven model of range evolution, with repeated intercontinental movements and regional radiations shaping present-day distributions.

The absence of a single-region origin, combined with the prevalence of composite ancestral ranges, suggests that early *Orthetrum* lineages occupied a connected Afro–Eurasian system, with subsequent lineage diversification structured by regional ecological and geographic factors. The timing of key divergences, including the early Miocene split of the Malagasy lineage (*Orthetrum azureum*), further highlights the importance of long-distance dispersal and independent colonization events in shaping island faunas.

Overall, these results reinforce the broader view that high dispersal capacity and ecological flexibility have played central roles in the evolutionary history of Odonata. By integrating phylogenomics, divergence time estimation and biogeographic modelling, this study provides new insights into the processes driving diversification in one of the most widespread dragonfly genera and establishes a robust framework for future comparative and evolutionary studies.

## AUTHOR CONTRIBUTIONS

**Violet Onsongo**: Conceptualization; methodology; investigation; formal analysis; data curation; visualization; writing—original draft. **Jessica Ware**: Conceptualization; supervision; funding acquisition; project administration; writing—review and editing. **John C. Abbott, Seth M. Bybee, Klaas-Douwe B. Dijkstra, Paul B. Frandsen, Aaron Goodman, Robert Guralnick, Vincent J. Kalkman, Manpreet Kohli, Lacie Newton, Lorenzo Prendini and Christopher J. Raxworthy**: Resources; writing—review and editing.

## ACKNOWLEDGEMENTS

We thank the Florida State Collection of Arthropods, particularly Bill Mauffray, and the Naturalis Biodiversity Center for the generous loan of material used in this study. We also thank Max Caspers for his work curating the Odonata collection at RMNH. We also thank the editor and three anonymous reviewers for their helpful comments and suggestions on our manuscript.

## FUNDING INFORMATION

The funding agency is the U.S. National Science Foundation (NSF). The grant title is Genealogy of Odonata (GEODE): Dispersal and Color as Drivers of 300 Million Years of Global Dragonfly Evolution. The NSF award numbers are Abbott: 2002489; Ware: 2002473; Bybee: 2002432; Guralnick: 2002457.

## CONFLICT OF INTEREST STATEMENT

The authors declare no conflict of interest.

## DATA AVAILABILITY STATEMENT

Raw anchored hybrid enrichment (AHE) sequencing reads have been deposited in the NCBI Sequence Read Archive (SRA) (https://www.ncbi.nlm.nih.gov/) under BioProject accession [PRJNA1475513]. All datasets associated with this study have been deposited in the permanent Dryad Digital Repository: https://doi.org/10.5061/dryad.4f4qrfjtf (Onsongo et al., 2026).

## ORCID

*Violet Onsongo* https://orcid.org/0009-0003-2738-8818
*John C. Abbott* https://orcid.org/0000-0002-6773-3976
*Seth M. Bybee* https://orcid.org/0000-0001-6224-6303
*Klaas-Douwe B. Dijkstra* https://orcid.org/0000-0002-5232-2277
*Paul B. Frandsen* https://orcid.org/0000-0002-4801-7579
*Aaron Goodman* https://orcid.org/0000-0002-7051-8249
*Robert Guralnick* https://orcid.org/0000-0001-6682-1504
*Vincent J. Kalkman* https://orcid.org/0000-0002-1484-7865
*Manpreet Kohli* https://orcid.org/0000-0002-3896-4513
*Lacie Newton* https://orcid.org/0000-0001-7269-6244
*Lorenzo Prendini* https://orcid.org/0000-0001-8727-7106
*Christopher J. Raxworthy* https://orcid.org/0000-0002-4517-0447
*Jessica Ware* https://orcid.org/0000-0002-4066-7681

## REFERENCES

Abbott, J.C., Bota-Sierra, C.A., Guralnick, R., Kalkman, V., González-Soriano, E., Novelo-Gutiérrez, R. et al. (2022) Diversity of Nearctic dragonflies and damselflies (Odonata). *Diversity*, 14, 575.

Boudot, J.-P., Monnerat, C., Juillerat, L., Feulner, G.R., Kunz, B., Corso, A. et al. (2020) Range, distribution, field identification, behaviour and exuvia description of *Orthetrum ransonnetii* (Odonata: Libellulidae). *Odonatologica*, 49, 199–244.

Breinholt, J.W., Earl, C., Lemmon, A.R., Lemmon, E.M., Xiao, L. & Kawahara, A.Y. (2018) Resolving relationships among the megadiverse butterflies and moths with a novel pipeline for anchored phylogenomics. *Systematic Biology*, 67, 78–93. Available from: https://doi.org/10.1093/sysbio/syx048

Burnham, K.P. & Anderson, D.R. (2004) Multimodel inference: understanding AIC and BIC in model selection. *Sociological Methods & Research*, 33, 261–304. Available from: https://doi.org/10.1177/0049124104268644

Bybee, S.M., Kalkman, V.J., Erickson, R.J., Frandsen, P.B., Breinholt, J.W., Suvorov, A. et al. (2021) Phylogeny and classification of Odonata using targeted genomics. *Molecular Phylogenetics and Evolution*, 160, 107–115. Available from: https://doi.org/10.1016/j.ympev.2021.107115

Camacho, C., Coulouris, G., Avagyan, V., Ma, N., Papadopoulos, J., Bealer, K. et al. (2009) BLAST+: architecture and applications. *BMC Bioinformatics*, 10, 421.

Capella-Gutiérrez, S., Silla-Martínez, J.M. & Gabaldón, T. (2009) trimAl: a tool for automated alignment trimming in large-scale phylogenetic analyses. *Bioinformatics*, 25, 1972–1973.

Chathura Priyadarshana, P.H.M.G., Warnakulasuriya Adriyan Sangilige, P.P.R., Opita Gamage, Y.D.G. & Hettiarachchige, C.J. (2023) Feeding behaviour of *Orthetrum sabina sabina* from Sri Lanka. *Zenodo*. Available from: https://doi.org/10.5281/zenodo.10156988

Clausnitzer, V., Kalkman, V.J., Ram, M., Collen, B., Baillie, J.E.M., Bedjanič, M. et al. (2009) Odonata enter the biodiversity crisis debate: the first global assessment of an insect group. *Biological Conservation*, 142, 1864–1869.

Corbet, P.S. (1999) *Dragonflies: behaviour and ecology of Odonata*. Ithaca, NY: Cornell University Press.

Cortés-Guzmán, D., Sinclair, J., Hof, C., Kalusche, J.B. & Haase, P. (2024) Dispersal, glacial refugia and temperature shape biogeographical patterns in European freshwater biodiversity. *Global Ecology and Biogeography*, 33, e13886.

De Marco, P. & Resende, D.C. (2002) Activity patterns and thermoregulation in a tropical dragonfly assemblage. *Odonatologica*, 31, 129–138.

Dijkstra, K.-D.B. (2025) *Dragonflies and damselflies of the world: a guide to their diversity*. Princeton: Princeton University Press.

Dijkstra, K.-D.B. & Clausnitzer, V. (2014) *The dragonflies and damselflies of eastern Africa*. Tervuren: Royal Museum for Central Africa.

Dijkstra, K.-D.B. & Kalkman, V.J. (2012) Phylogeny, classification and taxonomy of European dragonflies and damselflies (Odonata): a review. *Organisms Diversity & Evolution*, 12, 209–227. Available from: https://doi.org/10.1007/s13127-012-0080-8

Dijkstra, K.-D.B., Kalkman, V.J., Dow, R.A., Stokvis, F.R. & van Tol, J. (2014) Redefining the damselfly families: a comprehensive molecular phylogeny of Zygoptera (Odonata). *Systematic Entomology*, 39, 68–96. Available from: https://doi.org/10.1111/syen.12035

Dijkstra, K.-D.B., Kipping, J. & Mézière, N. (2015) Sixty new dragonfly and damselfly species from Africa (Odonata). *ZooKeys*. Available from: https://doi.org/10.5281/zenodo.35388

Dumont, H.J. & Verschuren, D. (2005) Odonata from the Ennedi and Ounianga regions of northern Chad. *Odonatologica*, 34, 291–297.

Ewels, P., Magnusson, M., Lundin, S. & Käller, M. (2016) MultiQC: summarize analysis results for multiple tools and samples in a single report. *Bioinformatics*, 32, 3047–3048. Available from: https://doi.org/10.1093/bioinformatics/btw354

Farkas, A., Jakab, T., Tóth, A., Kalmár, A.F. & Dévai, G. (2012) Emergence patterns of riverine dragonflies (Odonata: Gomphidae) in Hungary. *Aquatic Insects*, 34(Suppl. 1), 77–89. Available from: https://doi.org/10.1080/01650424.2012.643030

Futahashi, R. (2020) Diversity of UV reflection patterns in Odonata. *Frontiers in Ecology and Evolution*, 8, 201. Available from: https://doi.org/10.3389/fevo.2020.00201

Futahashi, R., Kato, Y., Watanabe, M., Tsuboi, M., Futahashi, R. et al. (2019) Molecular basis of wax-based color change and UV reflection in dragonflies. *eLife*, 8, e43045. Available from: https://doi.org/10.7554/eLife.43045

Futahashi, R., Kawahara-Miki, R., Kinoshita, M., Yoshitake, K., Yajima, S., Arikawa, K. et al. (2015) Extraordinary diversity of visual opsin genes in dragonflies. *Proceedings of the National Academy of Sciences of the United States of America*, 112, E1247–E1256.

Gillespie, R.G., Baldwin, B.G., Waters, J.M., Fraser, C.I., Nikula, R. & Roderick, G.K. (2012) Long-distance dispersal: a framework for hypothesis testing. *Trends in Ecology & Evolution*, 27, 47–56. Available from: https://doi.org/10.1016/j.tree.2011.08.009

Goodman, A., Frandsen, P.B., Ware, J.L., Tolman, E., Uche-Dike, R., Abbott, J. et al. (2023) Assessment of targeted enrichment locus capture across time and museums using odonate specimens. *Insect Systematics and Diversity*, 7, 5. Available from: https://doi.org/10.1093/isd/ixad011

Goodman, A., Frandsen, P.B., Ware, J.L. et al. (2025a) Systematic and taxonomic revision of emerald and tigertail dragonflies. *Systematic Entomology*. Available from: https://doi.org/10.1111/syen.70000

Goodman, A., Frandsen, P.B., Ware, J.L. et al. (2025b) Systematics and biogeography of the Holarctic dragonfly genus *Somatochlora*. *Systematic Entomology*, 50, 585–610. Available from: https://doi.org/10.1111/syen.12672

Goodman, A.M., Beatty, C.D., Büsse, S., Ubukata, H., Miyazaki, T., Blair, M.E. et al. (2024) Paleoecological niche modeling of Epiophlebia (Epiophlebioptera: Epiophlebiidae) reveals continuous distribution during the last glacial maximum. *International Journal of Odonatology*, 27, 60–76. Available from: https://doi.org/10.48156/1388.2024.1917262

Hadfield, R.K., Jordan, S.D., Polhemus, D.A., Sutherland, L.N., Peck, S.L., Abbott, J.C. et al. (2025) Diversification and evolution of Hawaiian *Megalagrion* damselflies (Pinapinao, Odonata: Coenagrionidae). *Systematic Entomology*, 51, 70,015.

Kalkman, V.J., Babu, R., Bedjanič, M., Conniff, K., Gyeltshen, T., Khan, M.K. et al. (2020) Checklist of the dragonflies and damselflies (Insecta: Odonata) of Bangladesh, Bhutan, India, Nepal, Pakistan and Sri Lanka. *Zootaxa*, 4849, 1–84. Available from: https://doi.org/10.11646/zootaxa.4849.1.1

Kalkman, V.J., Boudot, J.-P., Futahashi, R., Abbott, J.C., Bota-Sierra, C.A., Guralnick, R. et al. (2022) Diversity of Palaearctic dragonflies and damselflies (Odonata). *Diversity*, 14, 966.

Kalyaanamoorthy, S., Minh, B.Q., Wong, T.K.F., von Haeseler, A. & Jermiin, L.S. (2017) ModelFinder: fast model selection for accurate phylogenetic estimates. *Nature Methods*, 14, 587–589. Available from: https://doi.org/10.1038/nmeth.4285

Katoh, K. & Standley, D.M. (2013) MAFFT multiple sequence alignment software version 7: improvements in performance and usability. *Molecular Biology and Evolution*, 30, 772–780. Available from: https://doi.org/10.1093/molbev/mst010

Khelifa, R., Zebsa, R., Moussaoui, A., Kahalerras, A., Bensouilah, S. & Mahdjoub, H. (2013) Niche partitioning in three sympatric congeneric species of dragonfly, *Orthetrum chrysostigma*, *O. Coerulescens anceps* and *O. nitidinerve*: the importance of microhabitat. *Journal of Insect Science*, 13, 1–17. Available from: https://doi.org/10.1673/031.013.7101

Kohli, M., Letsch, H., Greve, C., Béthoux, O., Deregnaucourt, I., Liu, S. et al. (2021) Evolutionary history and divergence times of Odonata (dragonflies and damselflies) revealed through transcriptomics. *iScience*, 24, 103324. Available from: https://doi.org/10.1016/j.isci.2021.103324

Kück, P. & Meusemann, K. (2010) FASconCAT: convenient handling of data matrices. *Molecular Phylogenetics and Evolution*, 56, 1115–1118. Available from: https://doi.org/10.1016/j.ympev.2010.04.024

Lalṭanpuii, N., Senthil Kumar, N. & Mathai, M.T. (2014) Molecular and phylogenetic analysis of the genus *Orthetrum* (Odonata: Anisoptera: Libellulidae) using mitochondrial COI gene. *Science Vision*, 14, 152–157.

Larsson, A. (2014) AliView: a fast and lightweight alignment viewer and editor for large datasets. *Bioinformatics*, 30, 3276–3278.

Lemmon, A.R., Emme, S.A. & Lemmon, E.M. (2012) Anchored hybrid enrichment for massively high-throughput phylogenomics. *Systematic Biology*, 61, 727–744. Available from: https://doi.org/10.1093/sysbio/sys049

Matzke, N.J. (2013a) BioGeoBEARS: biogeography with Bayesian (and likelihood) evolutionary analysis in R scripts. Available at: http://cran.r-project.org/package=BioGeoBEARS

Matzke, N.J. (2013b) Probabilistic historical biogeography: new models for founder-event speciation, imperfect detection and fossils allow improved accuracy and model testing. *Frontiers of Biogeography*, 5, 242–248.

Matzke, N.J. (2022) Statistical comparison of DEC and DEC+J is identical to comparison of two ClaSSE submodels, and is therefore valid. *Journal of Biogeography*, 49(10), 1805–1824. Available from: https://doi.org/10.1111/jbi.14346

May, M.L. (1976) Thermoregulation and adaptation to temperature in dragonflies. *Ecological Monographs*, 46, 1–32.

Mendes, F.K. & Hahn, M.W. (2016) Gene tree discordance causes apparent substitution rate variation. *Systematic Biology*, 65, 711–721. Available from: https://doi.org/10.1093/sysbio/syw018

Minh, B.Q., Schmidt, H.A., Chernomor, O., Schrempf, D., Woodhams, M.D., von Haeseler, A. et al. (2020) IQ-TREE 2: new models and efficient methods for phylogenetic inference in the genomic era. *Molecular Biology and Evolution*, 37, 1530–1534. Available from: https://doi.org/10.1093/molbev/msaa015

Moore, M.P., Leith, N.T., Fowler-Finn, K.D. & Medley, K.A. (2024) Human-modified habitats imperil ornamented dragonflies less than their non-ornamented counterparts at local, regional and continental

scales. *Ecology Letters*, 27, e14455. Available from: https://doi.org/10.1111/ele.14455

Newton, L.G., Abbott, J.C., Bybee, S.M., Carter, P., Frandsen, P.B., Goodman, A. et al. (2026) Soaring systematics: an evaluation of biogeography and flight behaviour in dragonflies and damselflies (Insecta: Odonata) using phylogenomics. *Systematic Biology*. Available from: https://doi.org/10.1093/sysbio/syag005

Oertli, B. (2008) Use of dragonflies in the assessment and monitoring of aquatic habitats. In: *Dragonflies and damselflies: model organisms for ecological and evolutionary research*. Oxford: Oxford University Press.

Onsongo, V., Abbott, J.C., Bybee, S.M., Dijkstra, K.-D.B., Frandsen, P.B., Goodman, A. et al. (2026) Evolution and biogeography of the widespread dragonfly genus *Orthetrum* (Odonata: Anisoptera: Libellulidae): massive dispersal in the tertiary. *Dryad Digital Repository*. [dataset]. Available from: https://doi.org/10.5061/dryad.4f4qrfjtf

Paulson, D., Schorr, M., Abbott, J., Bota-Sierra, C., Deliry, C., Dijkstra, K.-D. B. et al. (2024) *World Odonata list*. Tuscaloosa, Alabama, USA: University of Alabama. Available from: https://www.odonatacentral.org/app/#/wol/ [Accessed 17th September 2024].

Paulson, D.R. (2009) *Dragonflies and damselflies of the west*. Princeton, NJ: Princeton University Press.

Prjibelski, A., Antipov, D., Meleshko, D., Lapidus, A. & Korobeynikov, A. (2020) Using SPAdes de novo assembler. *Current Protocols in Bioinformatics*, 70, e102. Available from: https://doi.org/10.1002/cpbi.102

Rambaut, A. (2014) FigTree v1.4.2: tree figure drawing tool. Available at: http://tree.bio.ed.ac.uk/software/figtree

Rambaut, A., Drummond, A.J., Xie, D., Baele, G. & Suchard, M.A. (2018) Posterior summarisation in Bayesian phylogenetics using tracer 1.7. *Systematic Biology*, 67, 901–904. Available from: https://doi.org/10.1093/sysbio/syy032

Ree, R.H. & Sanmartín, I. (2018) Conceptual and statistical problems with the DEC + J model of founder-event speciation and its comparison with DEC via model selection. *Journal of Biogeography*, 45, 741–749. Available from: https://doi.org/10.1111/jbi.13173

Ree, R.H. & Smith, S.A. (2008) Maximum likelihood inference of geographic range evolution by dispersal, local extinction and cladogenesis. *Systematic Biology*, 57, 4–14. Available from: https://doi.org/10.1080/10635150701883881

Ronquist, F. (1997) Dispersal–vicariance analysis: a new approach to the quantification of historical biogeography. *Systematic Biology*, 46(1), 195–203. Available from: https://doi.org/10.1093/sysbio/46.1.195

Suárez-Tovar, C.M., Guillermo-Ferreira, R., Cooper, I.A., Cezário, R.R. & Córdoba-Aguilar, A. (2022) Dragon colors: the nature and function of Odonata coloration. *Journal of Zoology*, 317, 1–9. Available from: https://doi.org/10.1111/jzo.12963

Subramanian, K.A., Emiliyamma, K.G., Babu, R., Radhakrishnan, C. & Talmale, S.S. (2018) *Atlas of Odonata (Insecta) of the Western Ghats*. Kolkata: Zoological Survey of India.

Suvorov, A., Jensen, N.O., Sharkey, C.R., Fujimoto, M.S., Bodily, P., Wightman, H.M.C. et al. (2017) Opsins have evolved under the permanent heterozygote model: insights from phylotranscriptomics of Odonata. *Molecular Ecology*, 26, 1306–1322. Available from: https://doi.org/10.1111/mec.13884

Suvorov, A., Scornavacca, C., Fujimoto, M.S., Bodily, P., Clement, M., Crandall, K.A. et al. (2022) Deep ancestral introgression shapes evolutionary history of dragonflies and damselflies. *Systematic Biology*, 71, 526–546. Available from: https://doi.org/10.1093/sysbio/syab063

Tang, X. & Wong, D.F. (2001) FAST-SP: a fast algorithm for block placement based on sequence pair. In: *Proceedings of the Asia South Pacific Design Automation Conference (ASP-DAC '01)*. New York, NY, USA: ACM Press, pp. 521–526. Available from: https://doi.org/10.1145/370155.370523

Tolman, E.R., Beatty, C.D., Bush, J., Kohli, M.K., Frandsen, P.B., Gosnell, J.S. et al. (2023) Exploring chromosome evolution in 250-million-year-old groups of dragonflies and damselflies (Insecta: Odonata). *Molecular Ecology*, 32, 5785–5797.

Tolman, E.R., Beatty, C.D., Kohli, M.K., Abbott, J., Bybee, S.M., Frandsen, P.B. et al. (2024) A molecular phylogeny of the Petaluridae (Odonata: Anisoptera): a 160-million-year-old story of drift and extinction. *Molecular Phylogenetics and Evolution*, 200, 108185. Available from: https://doi.org/10.1016/j.ympev.2024.108185

Ware, J.L., Pilgrim, E., May, M.L., Donnelly, T.W. & Tennessen, K. (2017) Phylogenetic relationships of north American Gomphidae and their close relatives. *Systematic Entomology*, 42, 347–358.

Ware, J.L. et al. (2025) Bringing shadowdragons to light: *Neurocordulia* systematics. *International Journal of Odonatology*, 28, 1–15. Available from: https://doi.org/10.48156/1388.2025.1917307

Wildermuth, H. (2008) Habitat requirements of *Orthetrum coerulescens*. *International Journal of Odonatology*, 11, 261–276. Available from: https://doi.org/10.1080/13887890.2008.9748328

Willink, B., Ware, J.L. & Svensson, E.I. (2024) Tropical origin, global diversification and dispersal in the pond damselflies (Coenagrionoidea) revealed by a new molecular phylogeny. *Systematic Biology*, 73, 290–307.

Yang, Z. (2007) PAML 4: phylogenetic analysis by maximum likelihood. *Molecular Biology and Evolution*, 24, 1586–1591.

Yong, H.S., Lim, P.E., Tan, J., Ng, Y.F., Eamsobhana, P. & Suana, I.W. (2014) Molecular phylogeny of *Orthetrum* dragonflies reveals cryptic species of *Orthetrum pruinosum*. *Scientific Reports*, 4, 5553.

Yong, H.S., Song, S.L., Suana, I.W., Eamsobhana, P. & Lim, P.E. (2016) Complete mitochondrial genome of *Orthetrum* dragonflies and molecular phylogeny of Odonata. *Biochemical Systematics and Ecology*, 69, 124–131.

Zhang, C., Rabiee, M., Sayyari, E. & Mirarab, S. (2018) ASTRAL-III: polynomial-time species tree reconstruction. *BMC Bioinformatics*, 19, 153. Available from: https://doi.org/10.1186/s12859-018-2129-y

Zhang, H. (2019) *Dragonflies and damselflies of China*, Vol. 2. Sofia: Pensoft.

## SUPPORTING INFORMATION

Additional supporting information can be found online in the Supporting Information section at the end of this article.

**Table S1.** Taxon assigned sampling regions for BioGeoBEARS.

**Table S2.** Species absent from this study, with their likely position within the phylogenetic tree based on morphology and biogeographical region.

**Table S3.** Probe set, AHE Loci recovered, Gap_ ambiguity and mean contig length.

**Table S4.** Gene concordance factor (gCF), site concordance factor (sCF) and quartet score statistics for all internal nodes in the *Orthetrum* phylogeny inferred from the concatenated maximum-likelihood analysis. Values are presented for each node together with the corresponding quartet frequencies and concordance categories, where values <30% indicate low concordance, 30%–60% indicate moderate concordance, and >60% indicate high concordance.

**Table S5.** BioGeoBEARS likelihoods under different biogeographic models with unconstrained analysis.

**Table S6.** BioGeoBEARS likelihoods under different biogeographic models with constrained_ *O. sabina*_ABC (Afro-Eurasian regions) _model comparison.

**Table S7.** BioGeoBEARS likelihoods under different biogeographic models under constrained_ *O. sabina*_DEF (Indo-Australasian regions) _model_comparison.

**Table S8.** Ancestral range probabilities under the unconstrained DEC model.

**Table S9.** Ancestral range probabilities under the DEF-constrained DEC model.

**Table S10.** Ancestral range probabilities under the ABC-constrained DEC model.

**Table S11.** Divergence time estimates for all nodes (59–115) in the *Orthetrum* chronogram, including node identity, crown or stem designation, mean age estimates (Ma), 95% highest posterior density (HPD) intervals and corresponding geological periods inferred from the MCMCtree analysis.

**Figure S1.** Supplementary maximum-likelihood (ML) phylogeny with branch lengths inferred from the concatenated anchored hybrid enrichment (AHE) dataset. Branch lengths are proportional to the estimated number of substitutions per site.

**Data S1.** Sequence alignments used for the phylogenetic analyses of Orthetrum.

**Data S2.** Input files and results for the BioGeoBEARS biogeographic analyses, including ancestral range reconstruction outputs.

**Data S3.** Input and output files used for divergence time estimation based on secondary calibrations.

**Data S4.** Files associated with the phylogenetic analyses, including partition files, tree files, and supporting analysis outputs.

**How to cite this article:** Onsongo, V., Abbott, J.C., Bybee, S.M., Dijkstra, K.-D.B., Frandsen, P.B., Goodman, A. et al. (2026) Evolution and biogeography of the widespread dragonfly genus *Orthetrum* (Odonata: Anisoptera: Libellulidae): Massive dispersal in the tertiary. *Systematic Entomology*, 51(3), e70066. Available from: https://doi.org/10.1111/syen.70066